

A real/fast-time simulator for impact assessment of spoofing & jamming attacks on GNSS receivers

Ivan Iudice*, Domenico Pascarella*, Gianluca Corraro[†], and Giovanni Cuciniello[†]

* Security of Systems and Infrastructures Laboratory, Reliability & Security Department

[†] Guidance, Navigation and Control Laboratory, Reliability & Security Department

Italian Aerospace Research Centre (CIRA), Capua (CE), Italy

Email: [i.iudice, d.pascarella, g.corraro, g.cuciniello]@cira.it

Abstract—In aviation, the impact of threats is becoming increasingly significant, particularly for global navigation satellite system (GNSS). Two relevant GNSS threats are represented by jamming and spoofing. In order to evaluate the technological solutions to counter GNSS attacks, such attacks should be assessed by means of a proper GNSS threat simulator. This work shows the implementation and the testing results of a GNSS security impact simulator which injects the desired threat scenarios as a deviations on the GNSS actual measurements. The proposed simulator can be integrated in both real- and fast-time simulation environments. The provided results confirm the effectiveness of the simulator, and include in-flight demonstrations by means of a flight experimental vehicle.

I. INTRODUCTION

A (cyber) threat represents any potential cause of a (cyber) security incident, where a security incident means an intentional event that might be, or could lead to, an operational interruption, disruption, loss, emergency, crisis, compromising integrity, availability or confidentiality in case of cyber impacts [1]. In aviation, the impact of threats is becoming increasingly significant. This is particularly true for *global navigation satellite system* (GNSS) since [2]: (i) its importance makes it an attractive target for attackers; (ii) its openness (at least for civil GNSS) makes it considerably vulnerable; (iii) its weak transmitting and receiving power makes it susceptible to interferences, both natural and malicious. Two relevant GNSS threats are represented by jamming and spoofing. *Jamming* refers to intentional transmission of *radio frequency* (RF) energy to hinder a navigation service by masking GNSS signals with interference. Instead, *spoofing* is a malicious interference made by a *spoofers* to alter a GNSS receiver measurement, providing fake position, velocity and time information.

In order to evaluate the technological solutions to counter GNSS attacks, such attacks should be assessed. Accordingly, a GNSS *Threat Simulator* (GTS) is an essential tool to: (i) characterize the impact of intentional attacks exploiting GNSS vulnerabilities; (ii) verify and validate GNSS intrusion detection and mitigation systems.

This work shows the implementation and the testing results of a GTS as a GNSS *security impact simulator*, i.e., a

simulator reproducing the desired threat scenarios by injecting representative deviations on the GNSS actual measurements. The simulator can be integrated in real/fast-time simulation testbeds for being used in a laboratory and flight environment in order to reproduce typical GNSS security threats in emulated/real GNSS receivers.

The provided results are referred to both fast-time and real-time simulations. For the latter, in-flight demonstrations of specific threat scenarios were performed by means of a flight experimental vehicle.

A. Related work

Several studies have addressed the characterization of commercial jammers and their effect on GNSS receivers. [3] compares theoretical predictions with experimental results to examine the effect of Gaussian interference on code tracking accuracy. [4] evaluates the effects of intrasystem and intersystem interference by analytical techniques based on established theory and first-order estimates, in terms of the receiver's effective carrier-to-noise-density ratio. In [5], the authors propose determining the minimum acceptable degradation of effective carrier-to-noise-density ratio, considering all receiver processing phases. [6] investigates the simulation, Kalman Filter tracking, and Kalman Filter geolocation of a chirp-type civilian GPS jammer. In [7], the impact of jammers on GPS and Galileo is investigated, showing that the signals of each system are affected in similar way.

About spoofing, [8] provides a preliminary risk assessment at system and aircraft level for potential cyberattacks to the Flight Management System and to GNSS receivers. [2] proposes a GNSS-induced spoofing simulation algorithm based on path planning, which generates spoofing signals by adjusting the related powers. [9] reports a general mathematical model of a received spoofed GNSS signal, considering the meaconing cyberattack. [10] analyses the impact of spoofing on the error covariance of the Inertial Navigation System (INS), revealing how the used Kalman filter responds to spoofing attacks. [11] reports the architecture of a platform for the simulation of GNSS threats, including spoofing and implementing enhanced models to better predict the occurrence of threats.

To the best of authors' knowledge, our work is the first to propose a joint real and fast-time simulator for impact assessment of spoofing and jamming attacks on GNSS receivers.

This paper falls under the activities carried out for the AURORA (Italian Urban aiR mObility technologies & distRibuted test-fAcility) project; this project has been funded by the European Space Agency under the NAVISP (NAVigation Innovation in Support Program) program, activity code NAVISP-EL3-018.

II. SYSTEM MODEL AND IMPLEMENTATION

The proposed GTS is composed by two modules: the RFI threats module and the Cyber threats module. The former is intended for injecting RFI threats by simulating intentional/unintentional interferences to the target GNSS receiver (e.g., jamming). The latter injects cyber attacks by simulating spoofing attacks to the target GNSS receiver.

A. Jamming model

Jamming includes GNSS attacks denying GNSS receivers the access to the information supplied by one or more GNSS satellites. Thus, jamming affects the availability feature of GNSS signals for the receivers [12].

In the RFI threats module of the proposed GTS, the interference impact is computed in terms of SNR gain. Different threat scenarios are simulated according to the nature of the interference, i.e., continuous or pulsed emissions. The SNR gain is generated as a composition of three distinct contribution: (i) continuous RFI (e.g., jamming, intersystem interferences), (ii) pulsed RFI (e.g., transponders, VHF radios), (iii) cyber threats (e.g., spoofing).

For the i -th satellite operating at the frequency f , the overall SNR gain is computed using the following expression,

$$G_{\text{RFI}}^{(i)}(f) \triangleq \frac{1 - \beta}{1 + \text{INR}_c(f) + \text{INR}_p(f, \beta) + \text{SPNR}_i(f)}, \quad (1)$$

where β represents the so-called *blanker* duty cycle,

$$\text{INR}_c(f) \triangleq \frac{\text{SNR}_{\text{max}}(f)}{\text{SIR}_c(f)}, \quad (2)$$

$$\text{INR}_p(f, \beta) \triangleq \frac{1}{\beta} \sum_{n=1}^{N_p} \frac{\text{SNR}_{\text{max}}(f)}{\text{SIR}_p^{(n)}(f)} d_n \quad (3)$$

$$\text{SPNR}_i(f) \triangleq \text{SNR}_i(f) \text{SSR}_i(f), \quad (4)$$

with $\text{SNR}_{\text{max}}(f)$ representing the maximum signal-to-noise power ratio, i.e., $\text{SNR}_{\text{max}}(f) \triangleq \max_i \text{SNR}_i(f)$, $\text{SIR}_c(f)$ standing for the overall signal-to-continuous-interference power ratio, $\text{SIR}_p^{(n)}$ and d_n corresponding to the signal-to-pulsed-interference power ratio and the duty-cycle, respectively, of the n -th pulsed interference, for all $n \in \{1, 2, \dots, N_p\}$, and, finally, $\text{SSR}_i(f)$ referring to the spoofing-to-signal power ratio of the i -th satellite (see Sec. II-B).

When the receiver is caught by the spoofing on the i -th satellite $\text{SNR}_i(f)$ and $\text{SPNR}_i(f)$ are swapped. Continuous/pulsed RFI and cyber threats follow different enabling path. Cyber threats enabling signal is provided by the spoofing module (see Sec. II-B). Regarding cyber threats, the simulation model assumes that the spoofing only affects the SNR of the satellite under attack; this assumption can be accepted given the (almost-)orthogonality of the chip sequences.

B. Spoofing model

Spoofing is a class of GNSS cyberattacks manipulating the information presented to GNSS receivers [13]. The only detectable differences between legitimate satellite signals and spoofed ones may be in discrepancies in timing, signal direction, strength, Doppler shift, and signal to noise ratio. As an example, the simplest form of spoofer is a *meaconer* which records authentic GNSS signals and plays back the recorded signals with a time delay and sufficient transmit power [12].

The spoofing impact is computed by the Cyber threats module of the proposed GTS in terms of pseudorange-drifts and spoofing-to-signal power ratios. For the computation of the pseudorange-drift, we extend the model available in [10], by evaluating the pseudorange $\rho_{i,r}(t)$ between a satellite i and a receiver r as,

$$\begin{aligned} \rho_{i,r}(t) &= c\tau_{i,r} + c[(t + \delta t_r) - (t + \delta t_i)] \\ &= c\tau_{i,r} + c(\delta t_r - \delta t_i), \end{aligned} \quad (5)$$

where c is the speed of light, $\tau_{i,r}$ is the signal transmission delay between i and r , δt_r is the receiver clock offset from the GNSS time scale, δt_i is the clock offset of the satellite from the GNSS time scale.

For an authentic signal from i , the signal delay $\tau_{i,r}^{(a)}$ may be modelled as,

$$\tau_{i,r}^{(a)} = \frac{d_{i,r}}{c} + I_{i,r} + T_{i,r}, \quad (6)$$

where $d_{i,r}$, $I_{i,r}$ and $T_{i,r}$ are the geometric range, the ionospheric delay and the tropospheric delay, respectively, between i and r . Then, the authentic pseudorange $\rho_{i,r}^{(a)}$ between i and r may be modelled as,

$$\rho_{i,r}^{(a)} = d_{i,r} + c(\delta t_r - \delta t_i) + cI_{i,r} + cT_{i,r}. \quad (7)$$

For a spoofed signal related to i and r by means of the spoofer s , the signal delay $\tau_{i,r}^{(s)}$ may be modelled as,

$$\tau_{i,r}^{(s)} = \frac{d_{i,s} + d_{s,r}}{c} + I_{i,s} + T_{i,s} + \Delta t_{s,\text{proc}}^{(i)} + \Delta t_{s,\text{ctrl}}^{(i)}, \quad (8)$$

where $d_{i,s}$ is the geometric range between the i and s , $d_{s,r}$ is the geometric range between s and r , $I_{i,s}$ is the ionospheric delay between i and s , $T_{i,s}$ is the tropospheric delay between i and s , $\Delta t_{s,\text{proc}}^{(i)}$ and $\Delta t_{s,\text{ctrl}}^{(i)}$ are the signal-processing delay and the signal-controlled delay, respectively, of s for i .

We assume that the atmospheric delays are the same for the receiver and the spoofer, so,

$$\begin{aligned} \tau_{i,r}^{(s)} &= \frac{d_{i,r} + (d_{i,s} + d_{s,r} - d_{i,r})}{c} + I_{i,r} + T_{i,r} \\ &\quad + \Delta t_{s,\text{proc}}^{(i)} + \Delta t_{s,\text{ctrl}}^{(i)} \\ &= \left(\frac{d_{i,r}}{c} + I_{i,r} + T_{i,r} \right) \\ &\quad + \left(\frac{d_{i,s} + d_{s,r} - d_{i,r}}{c} + \Delta t_{s,\text{proc}}^{(i)} + \Delta t_{s,\text{ctrl}}^{(i)} \right) \\ &= \tau_{i,r}^{(a)} + \Delta t_s^{(i,r)}, \end{aligned} \quad (9)$$

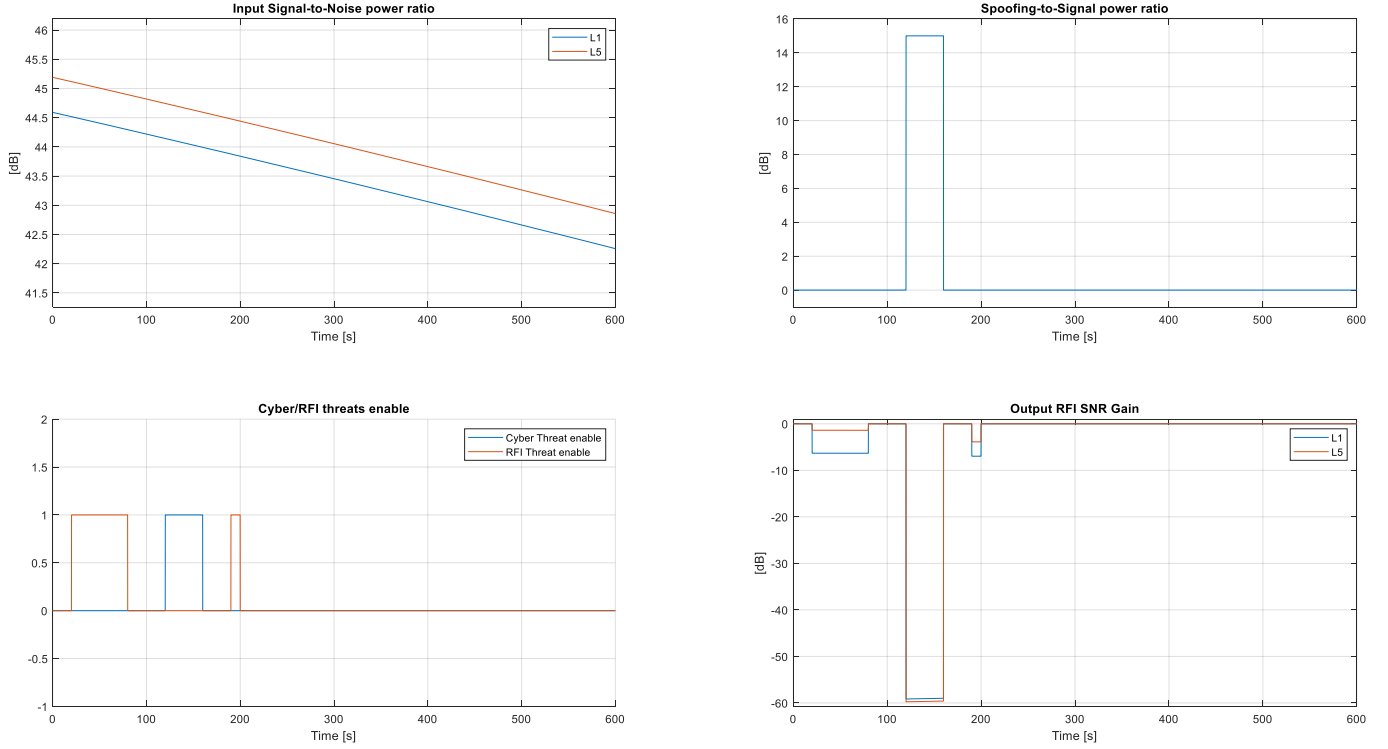


Fig. 1. RFI/Cyber Threat effects on PRN#19.

where,

$$\Delta t_s^{(i,r)} \triangleq \frac{d_{i,s} + d_{s,r} - d_{i,r}}{c} + \Delta t_{s,\text{proc}}^{(i)} + \Delta t_{s,\text{ctrl}}^{(i)}. \quad (10)$$

The term $\Delta t_s^{(i,r)}$ represents the spoofing signal delay. In general, we may assume that $\Delta t_{s,\text{proc}}^{(i)} = \Delta t_{s,\text{proc}}$. Moreover, the spoofer may exhibit a prediction capability of the navigation data bits of the authentic signal. Thus, this capability introduces a further offset $\delta t_{s,\text{pred}}$ to be considered in the spoofed pseudorange $\rho_{i,r}^{(s)}$, which may be modelled as,

$$\begin{aligned} \rho_{i,r}^{(s)} &= c\tau_{i,r}^{(s)} + c \left[(t + \delta t_r) - (t + \delta t_{s,\text{pred}} + \delta t_s^{(i)}) \right] \\ &= c\tau_{i,r}^{(a)} + c(\delta t_r - \delta t_i) + c\Delta t_s^{(i,r)} - c\delta t_{s,\text{pred}} \\ &= \rho_{i,r}^{(a)} + c\Delta t_s^{(i,r)} - c\delta t_{s,\text{pred}}. \end{aligned} \quad (11)$$

Note that the pseudorange-drift is actually produced if $\Delta t_s^{(i,r)} - \delta t_{s,\text{pred}}$ is less than the chip period of i . Furthermore, the spoofing model (11) holds in case the target receiver is single-frequency, instead, if the target receiver is multi-frequency, the model is extended as,

$$\rho_{i,r}^{(s)} = \frac{1}{1 - \gamma} \rho_{i,r}^{(s,L5)} - \frac{\gamma}{1 - \gamma} \rho_{i,r}^{(s,L1)}, \quad (12)$$

where $\rho_{i,r}^{(s,L5)}$ and $\rho_{i,r}^{(s,L1)}$ are the spoofed pseudoranges for L5 and L1 frequencies, respectively, according to (11), and $\gamma \triangleq \frac{f_{L1}^2}{f_{L5}^2}$, with f_{L1} and f_{L5} representing the corresponding carrier frequencies.

Regarding to the evaluation of $SSR_i(f)$, non-smart and smart spoofer scenarios are considered. For the former, the spoofer is simulated by applying a constant signal power. For the latter, the spoofer is simulated by applying a time-dependent spoofing power according to a specific control law, e.g., the reference signal power may be a ramp between a minimum and a maximum value in predefined time interval for all the spoofing signals. When the power reaches the maximum value, the receiver is locked by the spoofer. After the lock on a given spoofing signal, the spoofer keeps the maximum value of power.

C. GTS implementation

From a software point of view, the GTS model has been implemented in MATLAB/Simulink environment. It modifies the DFMC GNSS measurements in order to introduce the effects of (cyber) threats as described in the previous section. Such data are in input together with the *inertial measurement unit* (IMU) and *air data system* (ADS) measurements to the *hybrid navigation unit* (HNU) module, that implements all the algorithms for a tightly coupled GNSS/IMU/ADS sensor fusion with: autonomous *fault detection and exclusion* (FDE) of GPS/Galileo/BeiDou satellites; and estimation of navigation solution integrity/accuracy in terms of *protection level* (PL), and *figures of merit* (FoM). Finally, the output data are stored in a *flight data recorder* (FDR) for post-processing analysis.

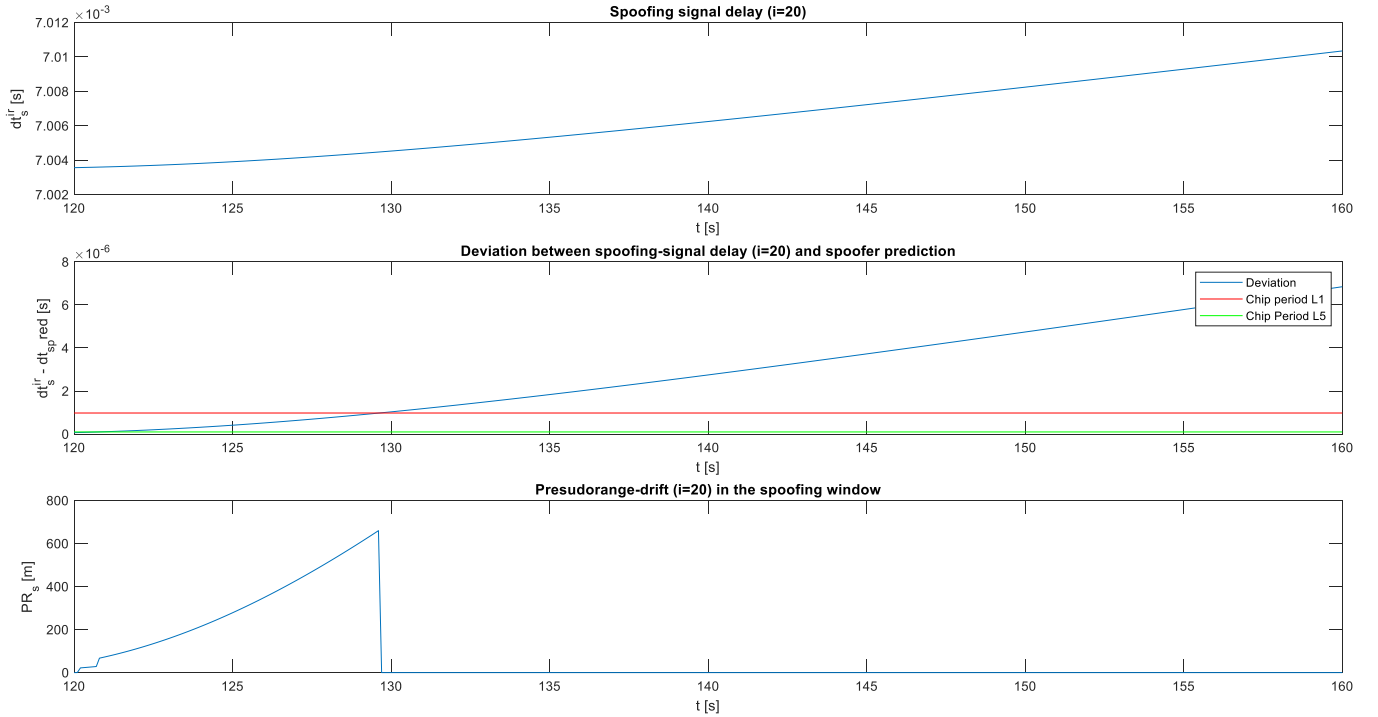


Fig. 2. Spoofing-signal delay and pseudorange-drifts of PRN#20.

III. TEST RESULTS

The GTS model was employed to validate a HNU for UAM applications, by means of both fast-time and *hardware-in-the-loop* (HIL) real-time simulations, and finally through in-flight demonstration.

A. Fast-time simulation results

In the fast-time simulation environment, the verification of the GTS and HNU modules has been performed following an architecture similar to the in-flight one shown in Fig. 3, implementing simulation models of on-board sensors and aircraft dynamics.

The fast-time simulation tests were carried-out on a time span of 10 min. Continuous interference was injected between 20 and 80 s, spoofing was injected between 120 and 160 s, finally, pulsed interference was injected between 190 and 200 s. For the continuous RFI threat was set a signal-to-interference power ratio of 50 dB and 60 dB for L1 and L5 bands, respectively. The spoofer was set in non-smart mode, with a spoofing-to-signal power ratio of 15 dB. Three pulsing interferences were considered, with all of them exhibiting a peak signal-to-interference power ratio of 40 dB and 45 dB in L1 and L5 bands, respectively, and 3%, 4%, and 5% as duty-cycle. The blanker duty-cycle of the receiver was disabled.

As you can see in Fig. 1, the first enabling window corresponds to the continuous interference which produces negative gains in both L1 and L2 bands. The second enabling window is related to spoofing; in this case the huge spoofing-to-signal

power ratio produces a relevant attenuation of the SNR. The third enabling window consists on the pulsed interferences; note that despite the power of pulsed sources quite greater than the continuous one, the overall effect on the SNR attenuation is almost the same of the continuous interference due to the pulsed nature of the interferences.

Regarding the spoofing, it also impacts the pseudorange estimates; thus, two other simulations were settled for non-smart and smart spoofer scenarios, both between 120 and 160 s. A static spoofer and a multi-frequency receiver were simulated. At the beginning of the spoofing window, the spoofer is 800 m far from the mobile target receiver. For the sake of brevity, here we report only the results in terms of pseudorange-drift, which are the same for both spoofing types, since these only affect the spoofing-to-signal power ratios and the receiver-lock status.

Fig. 2 shows: (i) the spoofing-signal delay; (ii) the deviation between the spoofing-signal delay and the spoofer prediction, i.e., $\Delta t_s^{(i,r)} - \delta t_{s,pred}$; (iii) the pseudorange-drift. As you can see, the deviation is always lower than the chip period of L5, except for an initial time interval; it is lower than the chip period of L1 until 130 s. As a consequence, the pseudorange-drift exhibits a first high-variation, i.e., when the deviation becomes greater than the chip period of L5. Then, the pseudorange-drift is cancelled when the deviation is greater than the chip period of L1, too, coherently with (12).

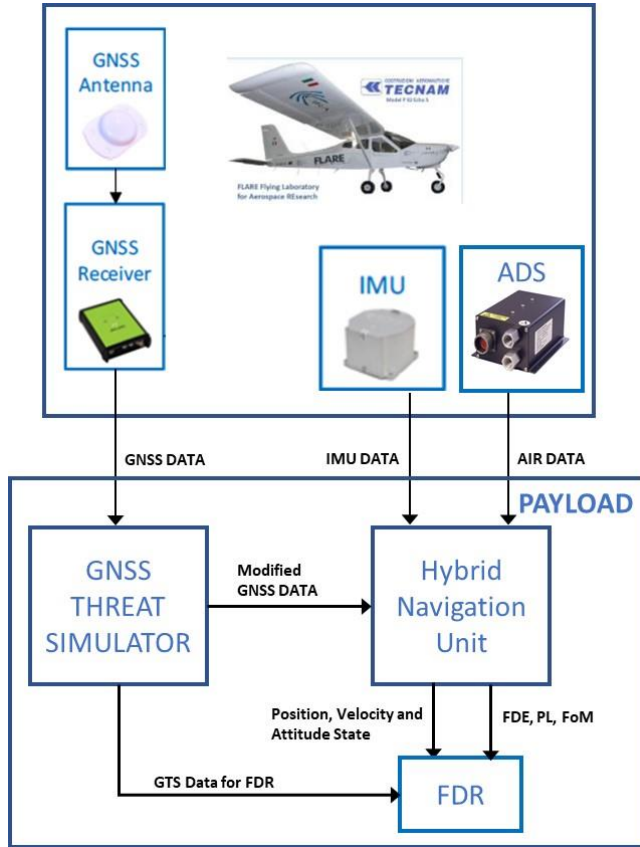


Fig. 3. In-flight test architecture.

B. Real-time flight results

The in-flight demonstrations were performed on a flight experimental vehicle based on a TECNAM P-92 ECHO S, modified in order to perform as a flying testbed for validation of autonomous flight technologies.

Fig. 3 depicts the architecture of the in-flight setup, with the following hardware devices:

- a GNSS receiver, model JAVAD-DELTA3, and related antenna capable to receive GPS, Galileo and BeiDou signals;
- an IMU, model Civitanavi Kryo, based on fiber-optic gyros and quartz accelerometers;
- an ADS;
- a PC-104 platform for the real-time execution of the items under test (i.e., GTS and HNU modules), not involved in the control of the automatic flight (payload module in Fig. 3).

In the in-flight demonstration campaign, two scenarios were tested using the GTS to simulate the impact of spoofing and jamming threats. Such simulations correspond to a static spoofing/jamming carried-on from the roof of a building located quite close to the flight trajectory and powered on

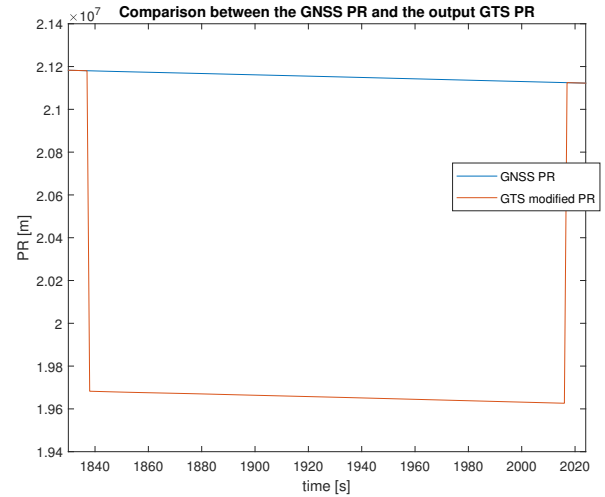


Fig. 4. Input and spoofed pseudoranges in real-time simulation.

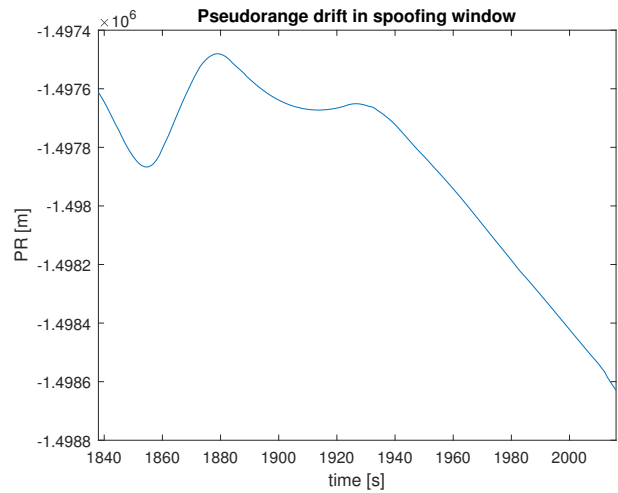


Fig. 5. Pseudorange drift in real-time simulation.

when the vehicle is proximal to the spoofer location, about < 4.5 km.

For spoofing, the GTS was configured to inject a meaconing ($\delta t_{s, \text{pred}} = 0$) attack with a spoofing-to-signal power ratio of about 45 dB, between 1838 and 2016 s. Fig. 4 shows the comparison between the input and spoofed pseudorange, whereas Fig. 5 reports the evaluated pseudorange-drift in the spoofing time window. The effect of the pseudorange drift changes with the distance between the spoofer and the receiver.

For jamming, the GTS was configured to inject a continuous RFI signal on both L1 and L5 bands, with a signal power such as to saturate the GNSS receiver RF section, between 2138 and 2279 s. The saturation caused the complete obscuration of satellites, until the vehicle was out of the effective range of the jammer. Fig. 6 depicts the effect of the simulated RFI threat on the SNR gain for one of the GPS satellite in view on both L1 and L5 bands.

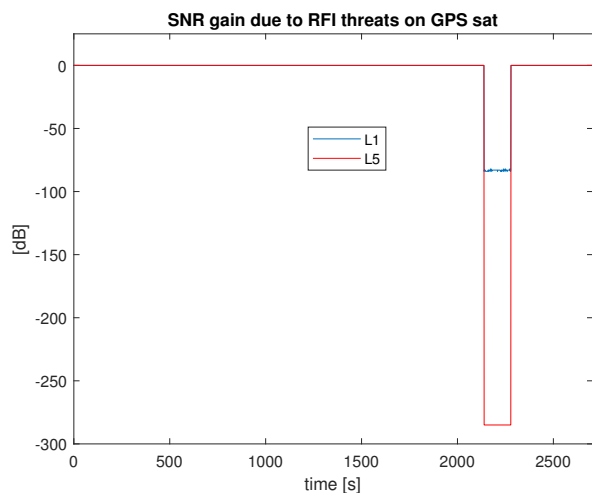


Fig. 6. SNR gain in real-time simulation.

IV. CONCLUSIONS

In this paper the implementation and testing results of a GTS as a GNSS *security impact simulator* are shown. The simulator can be integrated in real/fast-time simulation environments. It reproduces RFI and cyber (spoofing) threats in emulated/real GNSS receivers. The effectiveness of the GTS was proven by fast-time simulations, as well as by in-flight demonstrations of jamming and spoofing attack scenarios, carried-out by a flight experimental vehicle.

Future work will provide advanced models for smart spoofing scenarios, including control laws based on the real trajectory of the GNSS receiver. Furthermore, the GTS will be extended with lower level models in order to emulate the physical layer for both jamming and spoofing attacks.

REFERENCES

- [1] M. Le Fevre, B. Gözl, R. Flohr, T. Stelkens-Kobsch, and T. S. Verhoogt, "2.0 security risk assessment methodology for SESAR 2020; 02.00. 00," *SESAR Joint Undertaking: Brussels, Belgium*, vol. 25, 2017.
- [2] W. Wang and J. Wang, "GNSS induced spoofing simulation based on path planning," *IET Radar, Sonar & Navigation*, vol. 16, no. 1, pp. 103–112, 2022. [Online]. Available: <https://ietresearch.onlinelibrary.wiley.com/doi/abs/10.1049/rsn2.12167>
- [3] J. W. Betz, "Effect of narrowband interference on GPS code tracking accuracy," in *Proceedings of the 2000 National Technical Meeting of The Institute of Navigation*, 2000, pp. 16–27.
- [4] B. M. Titus, J. Betz, C. Hegarty, and R. Owen, "Intersystem and intrasystem interference analysis methodology," in *Proceedings of the 16th International Technical Meeting of the Satellite Division of The Institute of Navigation (ION GPS/GNSS 2003)*, 2003, pp. 2061–2069.
- [5] W. Liu, S. Li, L. Liu, M. Niu, and X. Zhan, "A comprehensive methodology for assessing radio frequency compatibility for GPS, galileo and compass," in *Proceedings of the 23rd International Technical Meeting of The Satellite Division of the Institute of Navigation (ION GNSS 2010)*, 2010, pp. 943–954.
- [6] R. H. Mitch, M. L. Psiaki, B. W. O'Hanlon, S. P. Powell, and J. A. Bhatti, "Civilian GPS jammer signal tracking and geolocation," in *Proceedings of the 25th International Technical Meeting of the Satellite Division of The Institute of Navigation (ION GNSS 2012)*, 2012, pp. 2901–2920.
- [7] D. Borio, C. O'Driscoll, and J. Fortuny, "Jammer impact on galileo and GPS receivers," in *2013 International Conference on Localization and GNSS (ICL-GNSS)*. IEEE, 2013, pp. 1–6.

- [8] R. M. Geister, J.-P. Buch, D. Niedermeier, G. Gamba, L. Canzian, and O. Pozzobon, "Impact study on cyber threats to GNSS and FMS systems," 2018.
- [9] M. Coulon, A. Chabory, A. Garcia-Pena, J. Vezinet, C. Macabiau, P. Estival, P. Ladoux, and B. Roturier, "Characterization of meaconing and its impact on GNSS receivers," in *Proceedings of the 33rd International Technical Meeting of the Satellite Division of The Institute of Navigation (ION GNSS+ 2020)*, 2020, pp. 3713–3737.
- [10] Y. Liu, S. Li, Q. Fu, and Z. Liu, "Impact assessment of GNSS spoofing attacks on INS/GNSS integrated navigation system," *Sensors*, vol. 18, no. 5, 2018. [Online]. Available: <https://www.mdpi.com/1424-8220/18/5/1433>
- [11] X. Zhao, X. Zhan, and K. Yan, "GNSS vulnerabilities: simulation, verification, and mitigation platform design," *Geo-spatial Information Science*, vol. 16, no. 3, pp. 149–154, 2013.
- [12] E. I. Adegoke, M. S. Bradbury, E. Kampert, M. D. Higgins, T. Watson, P. A. Jennings, C. R. Ford, G. Buesnel, and S. Hickling, "PNT cyber resilience : a lab2live observer based approach, report 1 : GNSS resilience and identified vulnerabilities. technical report 1," March 2020. [Online]. Available: <https://wrap.warwick.ac.uk/139519/>
- [13] D. Schmidt, K. Radke, S. Camtepe, E. Foo, and M. Ren, "A survey and analysis of the GNSS spoofing threat and countermeasures," *ACM Comput. Surv.*, vol. 48, no. 4, may 2016. [Online]. Available: <https://doi.org/10.1145/2897166>